European Polymer Journal 47 (2011) 614–629

Contents lists available at ScienceDirect

European Polymer Journal

journal homepage: www.elsevier.com/locate/europolj

Feature Article - Macromolecular Nanotechnology

Super-nucleation in nanocomposites and confinement effects on the crystallizable components within block copolymers, miktoarm star copolymers and nanocomposites

Alejandro J. Müller *, María Luisa Arnal, Mariselis Trujillo, Arnaldo T. Lorenzo

Grupo de Polímeros USB, Departamento de Ciencia de los Materiales, Universidad Simón Bolívar, Apartado 89000, Caracas 1080-A, Venezuela

ARTICLE INFO

Article history:
Available online 1 October 2010

Dedicated to Professor Nikos Hadjichristidis in recognition of his contributions to polymer science.

Keywords:
Block copolymers
Miktoarm star copolymers
Nanocomposites
Confined crystallization
Carbon nanotubes

ABSTRACT

In this paper we reexamine recent results obtained by our group on the crystallization of nanocomposites and linear and miktoarm star copolymers in order to obtain some general features of their crystallization properties. Different nanocomposites have been prepared where a close interaction between the polymer matrix and the nano-filler has been achieved: in situ polymerized high density polyethylene (HDPE) on carbon nanotubes (CNT); and polycaprolactone (PCL) and poly(ethylene oxide) (PEO) covalently bonded to carbon nanotubes. In all these nanocomposites a "super-nucleation" effect was detected where the CNTs perform a more efficient nucleating action than the self-nuclei of the polymer matrix. It is believed that such a super-nucleation effect stems from the fact that the polymer chains are tethered to the surface of the CNT and can easily form nuclei. For polystyrene (PS) and PCL block copolymers, miktoarm star copolymers (with two arms of PS and two arms of PCL) were found to display more compact morphologies for equivalent compositions than linear PS-*b*-PCL diblock copolymers. As a consequence, the crystallization of the PCL component always experienced much higher confinement in the miktoarm stars case than in the linear diblock copolymer case. The consequences of the topological confinement of the chains in block copolymers and nanocomposites on the crystallization were the same even though the origin of the effect is different in each case. For nanocomposites a competition between super-nucleation and confinement was detected and the behavior was dominated by one or the other depending on the nano-filler content. At low contents the super-nucleation effect dominates. In both cases, the confinement increases as the nano-filler content increases or the second block content increases (in this case a non-crystallizable block such as PS). The consequences of confinement are: a reduction of both crystallization and melting temperatures, a strong reduction of the crystallinity degree, an increase in the supercooling needed for isothermal crystallization, a depression of the overall crystallization rate and a decrease in the Avrami index until values of one or lower are achieved indicating a nucleation control on the overall crystallization kinetics.

1. Introduction

In recent years, polymeric materials (especially block copolymers and nanocomposites) have received substantial attention due to their especial morphology. They can organize in a great variety of fascinating solid state morphologies on the scale of micro and nanometers in the case of copolymers, or they can contain nano-fillers of different nature in the case of nanocomposites [1–15].

Copolymer synthesis offers the opportunity to control the size and morphology of the microdomains (MD's) by changing one or more parameters (molecular weight,

* Corresponding author. Tel./fax: +58 212 9063388.
E-mail address: amuller@usb.ve (A.J. Müller).

0014-3057 © 2010 Elsevier Ltd. Open access under CC BY-NC-ND license.
doi:10.1016/j.eurpolymj.2010.09.027

molecular architecture, molecular structure, segregation strength, composition and sample preparation) [5,16,17]. Also, a diversity of polymers with well-defined complex structures, such as star, graft and dendritic polymers have been synthesized using different pathways [16,17]. A variety of new macromolecules has been prepared thus far, many of them possessing interesting properties, in many cases distinctly different from their linear AB counterparts. Linear diblock and star block copolymers with crystallizable components offer an ideal way to produce model polymers for the study of the nucleation and crystallization events as a function of their morphology and chemical architecture [11,12,16–18]. The relationship between the structure and properties of many semi-crystalline block copolymers have been extensively studied [11,12,19–39] and reviewed [1–4]. Due to a chain crowding effect at the star junction point, the phase behavior and the domain spacing of neat miktoarm heteroarm star copolymers can differ considerably from those of linear AB diblock copolymers [40–49]. Thus, the higher stretching resistance of the arms in a miktoarm star block copolymer compared to analogous linear diblock copolymers is expected to produce important morphological differences as well as dramatic effects on the overall crystallization process [11,12].

On the other hand, carbon nanotubes (CNT) are considered excellent reinforcing fillers because of the outstanding properties that they can induce when adequately dispersed in polymeric matrices, such as elastic modulus increases without important reductions in ductility and dramatic enhancements in electrical conductivity. These properties are intimately connected with the extremely high aspect ratio of CNT which facilitate the establishment of percolation paths in the case of good dispersions [6–10,13–15]. Those properties of the nanocomposites are a strong function of the interface characteristics which in turn are determined by the superficial energy of the fillers. In the case of the CNT nano-fillers, because of their small size and high aspect ratio the percentage of atoms that are exposed on the interface can be as high as 50% of the total atoms in the nano-filler, this peculiar characteristic increases the superficial energy of the nano-fillers and favors a higher interaction between the filler and the matrix [50–54]. From the crystallization phenomenon point of view, the effect of the CNT on the nucleation and crystal growth of the semi-crystalline matrix can be found to be within on of these four cases: (i) a classical nucleation agent effect of CNT on the polymer matrix [55–65]. Increases in crystallization temperatures have been reported, thus an enhancement in nucleation density and in some cases reductions of crystallization times; (ii) no effect of CNT on the nucleation of polymer crystals has also been reported in some cases [66]; (iii) results that could be classified as anti-nucleation effects of CNT [67,68], where a reduction in nucleation density was clearly observed; and (iv) an exceptionally high nucleation effect induced by the CNT-polymer interface morphology, where the semi-crystalline polymer chains grow from the surface of CNT, increasing greatly the nucleation efficiency of the CNT upon the polymer crystallization phenomena [13–15].

This paper is dedicated to review the results of the recent collaboration of our group with that of Prof. Nikos Hadjichristidis (to whom this special issue is dedicated). We have reexamined our recent works on nanostructured materials (block copolymers and nanocomposites) in the light of other recent works by our group on nanocomposites (produced together with the collaboration of the group of Prof. Philippe Dubois in Belgium) in order to generate a global view of the effects of confinement experienced by the crystallizing phase upon the increase of the filler content (in nanocomposites) or a non-crystallizing covalently bonded block with different molecular architecture (in linear or miktoarm stars block copolymers).

2. Experimental section

2.1. Materials

The (PS_2)-*b*-(PCL_2) miktoarm star copolymers were synthesized in two steps, using high vacuum techniques and a heterofunctional initiator derived from pentaerythritol with two free and two protected –OH groups. One first step involved the esterification of the two unprotected hydroxyl groups with 2-bromoisobutyryl bromide followed by polymerization of styrene with the produced difunctional initiator. Deprotection of the two other –OH groups is carried out in a second step with subsequent ring opening polymerization (ROP) of ε-CL the presence of $Sn(Oct)_2$ to afford the final 4-miktoarm star. In a similar way, the linear PS-*b*-PCL block copolymers were also prepared in two steps including the ROP of ε-caprolactone (CL) with a 1-decanol/$Sn(Oct)_2$ initiating system, followed by the transformation of the end-OH group of PCL with 2-bromoisobutyryl bromide and polymerization of styrene with the newly formed Br-end groups. Details are given in a previous paper [11]. The molecular characteristics of the materials evaluated in this paper are provided in Table 1. In the notation: A_x-*b*-B_y^m here employed, the subscript numbers denote the mass fraction in weight percent and the superscripts give the number-averaged molecular weight M_n in kg/mol of the entire copolymer.

The hybrid materials MWNT-*g*-(PEO) (with a 9.5 wt.% MWNTs) and MWNT-*g*-PCL (with a 2 wt.% MWNTs) used for this study were synthesized as described in our previously reported work [15], and for comparison analogous PCL (M_n of 27 kg/mol, polydispersity of 1.07) and PEO (M_n of 29 kg/mol, polydispersity of 1.2) homopolymers were chosen.

The HDPE/CNT nanocomposites were prepared by a soft method derived from the polymerization-filling technique (PFT) using metallocene catalysis. Methylaluminoxane (MAO), a well-known co-catalyst used in metallocene-based olefin polymerization process, was anchored onto the surface of CNT in suspension in dried heptane. The metallocene catalyst employed here was bis(pentamethyl-η^5-cyclopentadienyl)zirconium(IV) dichloride $(Cp_2^*)ZrCl_2$, where Cp* where Cp stands for cyclopentadienyl), which was then reacted with the surface-activated carbon nanotubes. The addition of ethylene yields the synthesis of polyethylene (HDPE) exclusively at the surface of the CNT. Detailed description of the polymerization process is presented in Refs. [13,14]. Table 2 summarized the compositions of the HDPE/CNT samples evaluated.

Table 1
Molecular characteristics of the (PCL_2)-*b*-(PS_2) miktoarm star and PCL-*b*-PS linear block copolymers. Adapted from Ref. [11,12].

Sample	PCL	PCL-*b*-PS diblock copolymers			χN[d]
	M_n[a] $\times 10^{-3}$	M_w/M_n[a]	wt.% εCL[b]	M_n[c] x10^{-3}	(25 °C)
PCL_{80}-*b*-PS_{20}^{36}	30	1.7	79.8	36.1	8.4
PCL_{41}-*b*-PS_{59}^{73}	30	1.35	41.2	72.8	16.8
PCL_{20}-*b*-PS_{80}^{153}	30	1.46	19.6	152.8	38.4
	(PCL_2)	(PCL_2)-*b*-(PS_2) miktoarm block copolymers			
$(PCL_2)_{72}$-*b*-$(PS)_{34}^{28}$	24.5	1.15	71.8	34.2	7.1
$(PCL_2)_{39}$-*b*-$(PS)_{61}^{62}$	24.5	1.18	39.3	61.8	14.3
$(PCL_2)_{27}$-*b*-$(PS)_{73}^{100}$	24.5	1.41	27.1	100.1	25.6

[a] By size exclusion chromatography in THF at 40 °C.
[b] By ^{1}H NMR spectroscopy in $CDCl_3$ at 25 °C.
[c] Calculated by the molecular weight of the (PCL_2) or PCL macroinitiator and the composition by ^{1}H NMR.
[d] The Flory–Huggins enthalpic segmental interaction parameter, χ, was calculated using the following equation: $\chi_{PCL/PS}(T) = 7.4322/T$.

Table 2
HDPE/CNT nanocomposites evaluated: HDPE/SWNT ($PE_xS_yA_z$), HDPE/DWNT ($PE_xD_yA_z$), HDPE/MWNT ($PE_xM_yA_z$). Adapted from Ref. [13,14].

Samples	CNT type	Composition (in wt.%) CNT/HDPE/Al_2O_3
HDPE	–	0.00/92.40/7.60
$PE_{87}S_8A_5$	SWNT	7.57/87.07/5.36
$PE_{56}S_{20}A_{24}$	SWNT	20.05/56.08/23.87
$PE_{33}S_{36}A_{31}$	SWNT	33.21/36.21/30.58
$PE_{82}D_8A_{10}$	DWNT	7.60/82.20/10.17
$PE_{60}D_{17}A_{23}$	DWNT	17.35/60.16/22.49
$PE_{44}D_{26}A_{30}$	DWNT	26.19/43.45/30.49
$PE_{83}M_6A_{11}$	MWNT	5.91/82.55/11.53
$PE_{68}M_{11}A_{21}$	MWNT	11.15/68.21/20.64
$PE_{41}M_{26}A_{33}$	MWNT	26.41/41.06/32.53

2.2. Techniques

2.2.1. Differential scanning calorimetry (DSC)

Samples of approximately 2–5 mg were encapsulated in aluminum pans and measured in a Perkin–Elmer Pyris 1 calibrated with Tin and Indium under high purity nitrogen atmosphere. The thermal protocols employed are described below.

2.2.1.1. Standard DSC experiments. In the standard DSC dynamic experiments the DSC scans were obtained at 10 or 20 °C/min. All DSC cooling curves were recorded after the samples were held in the melt (at least 30 °C above the sample peak melting temperature) for 3 min in order to erase all previous crystalline history of the semi-crystalline component. The crystallization and melting enthalpies values were normalized with respect to the semi-crystalline fraction within the samples.

2.2.1.2. Isothermal DSC experiments. In the isothermal crystallization experiments the samples were held in the melt (at least 30 °C above the sample peak melting temperature) for 3 min in order to erase all previous crystalline history, and then quickly cooled (at 60 °C/min) to the desired crystallization temperature (T_c) where the isothermal DSC scan was recorded. Before performing the definitive isothermal crystallization experiments, tests were performed to ensure that the samples did not crystallize during cooling to T_c by immediately heating the samples when the temperature reached the desired T_c; if any melting occurred, then it was concluded that the crystallization took place during cooling and the isothermal experiment was not performed at that T_c. This procedure, for finding the ideal first T_c, was repeated (after erasing the crystalline history by keeping the sample 3 min in the melt), until no crystallization during cooling was evident.

When the semi-crystalline component content was low (or its crystallization was strongly restricted) in the sample (usually below 30 wt.%) the conventional isothermal kinetics were beyond the resolution of the DSC (i.e., the amount of heat evolved per unit time was too small to be measured isothermally). The isothermal crystallization was performed instead by "isothermal step crystallization" [32]. This procedure was performed following the guidelines of our previous work [32]: (a) erasure of crystalline history; (b) fast cooling (60 °C/min) down to T_c; (c) the sample was held at T_c for a time t_c, which was later increased in the subsequent steps; (d) heating at 10 °C/min from T_c to the molten state. The heat of fusion calculated from this DSC heating scan should correspond to the crystallization enthalpy of the crystals formed during step "c" at T_c for the specified crystallization time; (e) steps (a–d) were repeated employing the same T_c in step "b", but at increasing t_c. The final t_c was taken as the time when the melting enthalpy in the subsequent heating scan did not change with respect to the previous one; (f) the whole process was repeated for different T_c temperatures.

2.2.1.3. Self-nucleation experiments (SN). The self-nucleation and annealing experiment using DSC was originally applied by Fillon et al. [69] to isotactic polypropylene (PP). It has been applied by our group to the study of several materials including block copolymers [70–73]. These experiments involved the partial melting of a crystalline "standard" state followed by recrystallization using as nuclei the crystal fragments produced in the partial melting stage. The detailed procedure used here is described as follows: (a) erasure of any previous crystalline history by heating the sample up to 30 °C above its peak melting temperature (T_1) for 3 min; (b) creation of a "standard" crystalline history by cooling at a rate of 20 °C/min to −20 °C. This

step ensures that the crystallization of the polymer under investigation occurs at the same dynamic conditions; (c) heating at 20 °C/min up to a self-nucleation temperature (T_s). (d) The thermal conditioning at T_s is performed for five minutes. (e) DSC cooling scans from T_s until −10 °C at a rate of 20 °C/min, where the effects of the thermal treatment will be reflected on the crystallization of PE, and (f) DSC heating scans from −10 to T_1, where the effects of the entire thermal treatment will also be reflected in the melting of the crystallizable component. Depending on T_s, selected for step (d) and according to Fillon et al. [69], the sample will be: *completely molten:* If T_s is too high, no self-nuclei or crystal fragments can survive, and the sample is said to be in *Domain I* or complete melting domain. *Self-nucleated:* When T_s is high enough to melt the sample almost completely, but low enough to leave active self-nuclei (Fillon et al. [69] proposed that the self-nuclei are crystal fragments, however, more recently we have proposed that such self-nuclei could be composed of crystallization precursors or by molecules that retain crystalline memory of the material, i.e., local segmental orientation [74]) the crystallization peak shifted to higher temperatures during the subsequent cooling from T_s, the sample is said to be in *Domain II*, or the self-nucleation domain. *Self-nucleated and annealed:* When T_s is too low, only some of the crystals will melt. Therefore, the unmolten crystals will be annealed during the five minutes at T_s, while the rest of the polymer will be self-nucleated during the subsequent cooling from T_s. The sample, in such cases, is said to be in *Domain III* or the self-nucleation and annealing domain. If annealing took place at T_s, then a second, higher melting peak might be observed.

2.2.2. Transmission electron microscopy (TEM).

The bulk morphology of the copolymers was examined by bright field TEM using a JEOL 1220 operated at 100 kV. Films of approximately 1 mm thick were prepared by casting from a 3 wt.% solution of the sample in toluene at 70 °C in order to avoid gelation upon solvent evaporation. After complete evaporation of the solvent (ca. 3–4 days), the films were kept at 120 °C for 15 h in order to improve the morphological segregation; next these samples were allowed to cool slowly to room temperature (at approximately 0.1 °C/min) in order to allow for maximum crystallization of the semi-crystalline component. Thin sections were cut at −130 °C using a LEICA EMFCS ultramicrotome equipped with a diamond knife. Staining of the copolymers was accomplished by exposing thin sections to RuO_4 (preferential staining of the amorphous PS component).

Also, the HDPE/CNT morphological observations were performed using this instrument. Lamellar thicknesses measurements were performed on micrographs taken after samples were isothermally crystallized for 7 days at 124 °C. They were after embedded in resin and cut with a diamond knife, those thin sections thus obtained were stained with RuO_4 vapors.

For the PEO and PCL MWNTs grafted materiales, TEM analysis was performed using a Hitachi H-800 TEM operating with an accelerating voltage of 100 kV. Samples were prepared by dropping a ~5 μL solution on a freshly glow discharged carbon film supported by a 400 mesh Cu grid.

3. Results and discussion

3.1. Morphology

In this study two analog sets (in wt.% composition) of PCL-containing copolymers are compared. The $(PCL)_2$-*b*-$(PS)_2$ miktoarm star block copolymers have χN values (where χ is the Flory–Huggins interaction parameter and N, the degree of polymerization of the block copolymer) in the range between 7.1 and 25.6 (at room temperature) that indicate a behavior in between total miscibility of both blocks (χN lower than 10) and a weakly-segregated regime (especially for $\chi N = 25.6$). In the second case, the linear PCL-*b*-PS system has slightly higher χN values between 8.4 and 38.4 (at 25 °C). Fig. 1 shows selected TEM micrographs for PCL-*b*-PS linear diblock copolymers and for (PCL_2)-*b*-(PS_2) miktoarm star block copolymers. For the diblock copolymers (Fig. 1A and C) the morphologies obtained are expected on the basis of their composition (i.e., lamellae for the diblock with 41% PCL and PCL cylinders for that with 20% PCL) for segregated diblock copolymers as it has been reported in the literature [1–5].

In the case of miktoarm star block copolymers where phase segregation in the melt was encountered (Fig. 1B and D), the morphology obtained was quite different from that observed for their linear analogs. The TEM micrograph for the $(PCL_2)_{39}$-*b*-$(PS_2)_{61}^{62}$ miktoarm copolymer (Fig. 1B) exhibits a cylindrical morphology with a clear hexagonal array of PCL cylinders. Additionally, the SAXS profiles for this miktoarm star copolymer are displayed next to Fig. 1B. A scattering peak at 120 °C (when the sample is in the melt) confirms that the copolymer undergoes phase segregation in the melt state. The diameter of the cylindrical microdomains calculated from the form factor position was approximately 38 nm which closely agrees with that estimated from the TEM micrograph (41 nm). For the $(PCL_2)_{27}$-*b*-$(PS_2)_{73}^{100}$ miktoarm sample, TEM revealed a morphology constituted by PCL spheres in a PS matrix (see Fig. 1D). From the SAXS profiles for this copolymer, the position of the form factor peak prescribed the radius of the spherical microdomains equal to 14.2 nm, again in a good agreement with the value calculate from the TEM micrographs (16 nm) [11,12].

Fig. 1 shows that the morphologies are more confined for the PCL component in the miktoarm star copolymers than expected on the basis of the composition as compared to their linear diblock copolymer analogs. This allowed us to speculate that the segregation strength within the miktoarm star block copolymers is stronger than that exhibited by the corresponding linear diblocks at similar PCL contents. The observation of a clear hexagonally-packed cylindrical morphology by TEM in the miktoarm star block copolymer $(PCL_2)_{39}$-*b*-$(PS_2)_{61}^{62}$ (Fig. 1A) in spite of its approximately 0.39 volume fraction of PCL is peculiar since for such a composition lamellar microdomains (Fig. 1A) are observed for its linear diblock copolymer analog. This behavior was explained taking into consideration

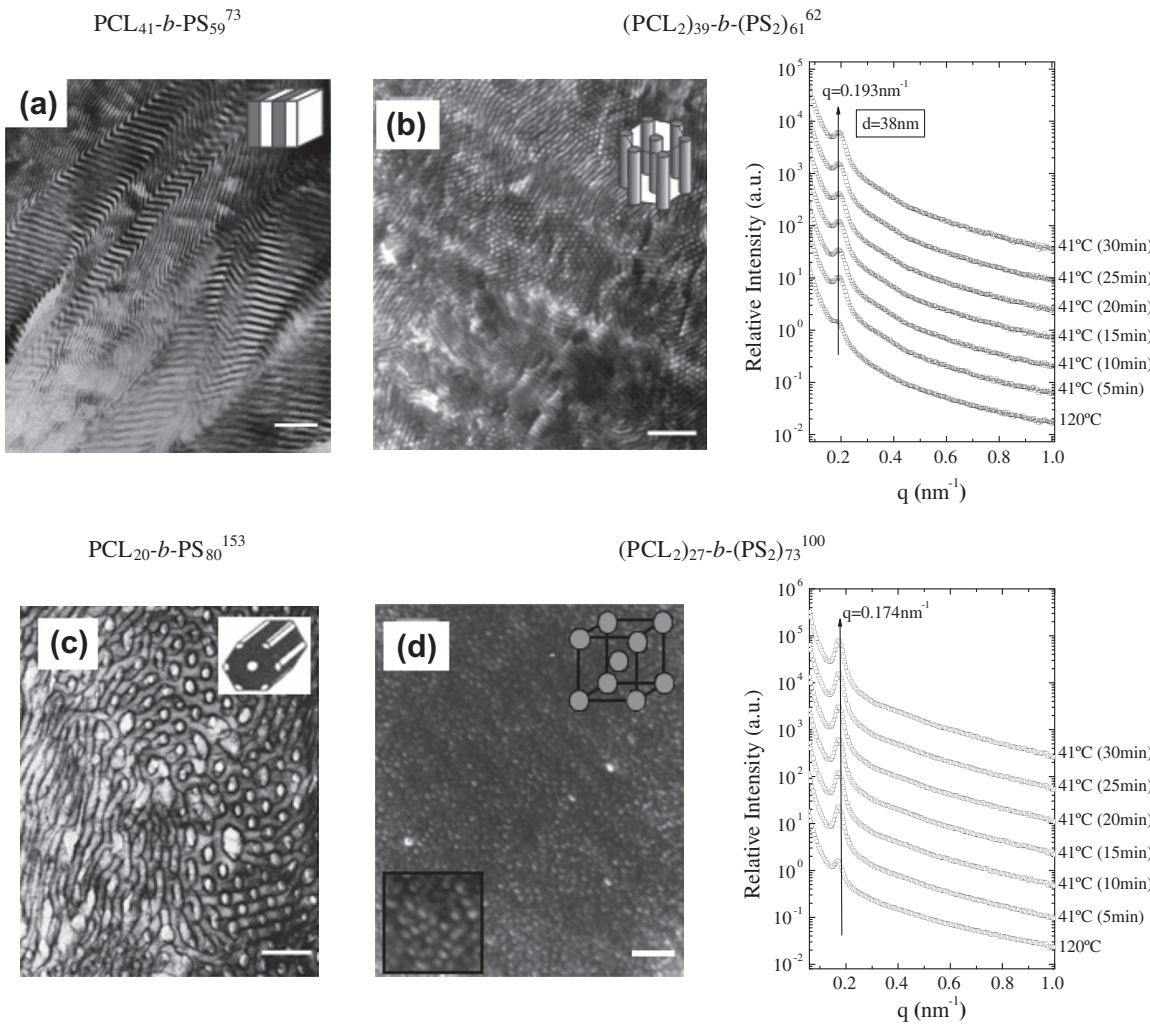

Fig. 1. TEM micrographs and SAXS scattering profiles of selected linear PCL-*b*-PS diblock copolymers (scale bar: 100 nm) and of the (PCL_2)-*b*-(PS_2) miktoarm star copolymers (scale bar: 200 nm). The copolymers were stained with RuO_4 (PS component is gray). Adapted from Refs. [11,12].

previous theoretical predictions for star copolymers [40,41]. These previous works have claimed that different morphologies could be expected because of the higher resistance of the arms to be stretched in a miktoarm star copolymer as compared to a linear one, and the relative strong dependence of the phase boundaries on the number of each type of arm [11,12,40,41].

Fig. 2 shows TEM micrographs of selected MWNT containing materials. In Fig. 2a, a distinct core–shell structure with MWNTs at the center and a thin layer around the MWNTs with varying thickness (average 25 nm) for the MWNT-*g*-PEO sample can be observed, since the large MWNT bundles originally present in the sample were separated during polymerization after being covered with the polymer layer due to the repulsion between the different polymer chains [15].

Fig. 2b, shows a micrograph of the $PE_{41}M_{26}A_{33}$ nanocomposite where a thin coating of HDPE can be seen surrounding the CNT's, confirming previous results on the same type of material [13,14]. Fig. 2c shows the lamellar morphology surrounding the MWNT's in $PE_{83}M_6A_{11}$, after a prolonged isothermal crystallization (1 week at 124 °C). The lamellae grew from the CNT surface in a direction roughly perpendicular to the CNT main axis, creating a bottle brush like morphology [13,14,55,59]. This peculiar morphology is derived from the strong nucleation effect that the MWNT create on the PE, especially because of the in situ polymerization procedure (i.e., the PE chains grow from the surface of the CNT and are therefore ideally positioned to become nucleated by its surface). Evidences of this nucleation effect are presented below.

3.2. Thermal characterization by DSC

Previous references have discussed in detail DSC cooling and heating scans of the nanostructured block copolymers presented here [11,12] and of the nanocomposites [13–15]. Therefore we will concentrate here in the analysis of the thermal transition temperatures obtained. Fig. 3 shows the melting and crystallization peak temperatures (T_m

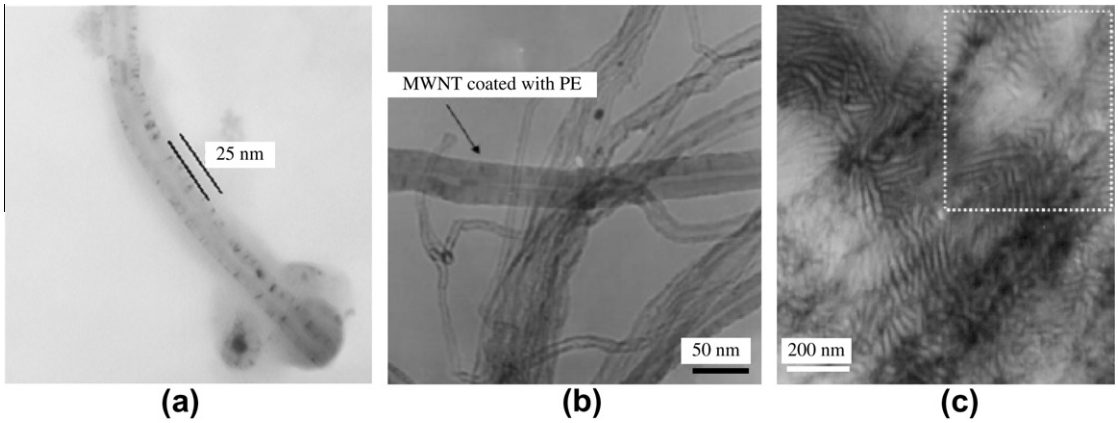

Fig. 2. TEM images of (a) MWNT-*g*-PEO; (b) MWNT coated with PE final composition $PE_{41}M_{26}A_{33}$; (c) $PE_{83}M_6A_{11}$; after isothermal crystallization for 1 week at 124 °C. Adapted from Refs. [13–15].

and T_c) temperatures and the crystallinity degree (%X_c) for the PCL-containing copolymers (linear diblocks and miktoarm stars).

The PCL homopolymer samples (with a M_n of 29 kg/mol) exhibits a T_c and T_m of 31.5 and 56.8 °C, respectively. Fig. 3a demonstrates that as morphological confinement increases the values of T_c and T_m also decrease [11,12]. The decrease in the melting temperature (and in the %X_c, see Fig. 3b) indicates that the previous crystallization process was greatly affected by the composition of each copolymer (i.e., as confinement increased, it occurred at higher supercoolings, where thinner lamellar crystals that melt at lower temperatures were produced). The chains topological confinements increased as a result of the decreased MD dimensions and larger surface area of the MD's (on going from lamellae to cylinders and finally to spheres).

Fig. 3 also compares the behavior of the miktoarm stars with the linear diblock copolymer analogs. It is evident that both crystallization and melting temperatures, and crystallinity degrees are smaller for the PCL phase within the miktoarm stars than within the linear diblock copolymers at equivalent compositions thus indicating a higher degree of confinement for the miktoarm star block copolymers. The confinement caused by the miktoarm molecular architecture is so large, that even comparing similar morphologies with their linear counterparts (at different compositions) a greater depression in T_c, T_m and X_c is obtained.

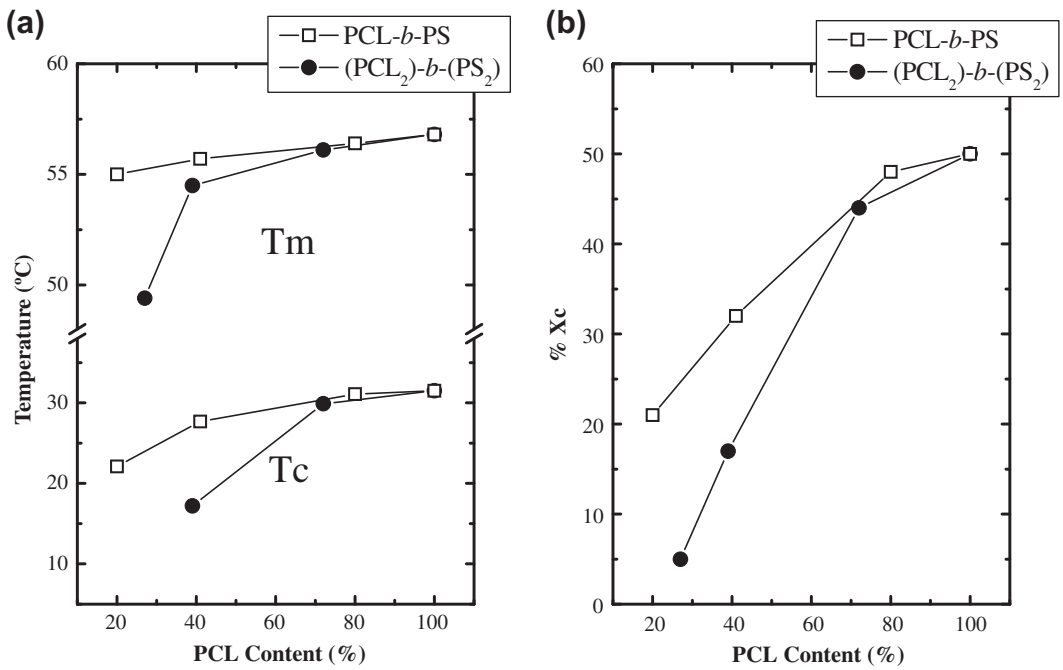

Fig. 3. (a) Crystallization (T_c) and melting peak temperatures (T_m) and (b) crystallinity degree, for linear PCL-*b*-PS diblock copolymers and (PCL_2)-*b*-(PS_2) miktoarm star copolymers as function of PCL content.

For example, if we compare the two cylinder forming samples of Fig. 1 in Fig. 3, the values of T_c, T_m and X_c are all much smaller for the miktoarm star copolymer $(PCL_2)_{39}$-*b*-$(PS_2)_{61}^{62}$ than for the linear diblock copolymer sample PCL_{20}-*b*-$(PS_2)_{80}^{153}$, even though the first one contains 39% PCL and the second one only 20%.

Fig. 4 summarizes the thermal behavior exhibited by all the in situ polymerized HDPE/CNT nanocomposite samples. Values presented in those graphs include the T_c determined during cooling from the melt at 10 °C/min, the T_m recorded during a subsequent heating DSC scan at 10 °C/min and the degree of crystallinity ($\%X_c$) obtained after cooling the sample from the melt. The results shown in Fig. 4 clearly indicate that: (i) regardless of the CNT nature (single, double or multiwall) a strong nucleation effect is produced on the HDPE matrix as revealed by the increase in T_c; (ii) the crystals produced are thermodynamically more stable in the in situ polymerized nanocomposites as compared to neat HDPE as indicated by their higher melting points; (iii) the degree of crystallinity decreases as the amount of CNT increases. It could be noted how the decrease in crystallinity is much more pronounced at higher CNT concentrations, where the presence of high contents of CNT probably interferes with crystal growth, especially when the extremely high number of nucleating sites they provide are taken into account; and (iv) when CNT content increases the amount of Al_2O_3 residues also increases, hence the HDPE/CNT composite will behave as a material with a PE phase of only 30–50 wt.% of the sample and a high load of fillers (both CNT and alumina), thus a confinement effect will be produced.

The remarkable trend observed in Fig. 4a indicates a competition between the super-nucleation effect caused by the CNT's and the confinement effect they also produced on the HDPE matrix. Therefore at low CNT's content, the nucleation effect dominates and a sharp increase in T_c and T_m is observed. However as the content of CNT's is larger than about 7% the confinement effect seems to dominate and a maximum in the plot of Fig. 4a can be observed in most cases. The confinement effect will depend on the interaction between the CNT surface and the HDPE chains which are nucleated at their surface. Therefore it is expected that the larger the surface area of CNT the higher the confinement effect. Fig. 4b illustrates this effect since at higher CNT's content the reduction in crystallinity is a function of the CNT type employed. The confinement effect in terms of reduction of $\%X_c$ increases in the order MWNT, DWNT and SWNT. For the same CNT content the surface area of CNT should increase in precisely the same order.

The comparison of Figs. 3 and 4 allow us to conclude that in both cases, the decrease of the crystallizing phase content can produce confinement effects that produce similar effects: a reduction in T_c, T_m and $\%X_c$. In one case the confinement is due to the change in MD morphology combined with the change in molecular architecture (when stars are compared to linear diblock copolymers) while in the other the confinement is related to the increase in the surface area of the nano-filler. We will demonstrate below that these confinement effects can also affect the crystallization kinetics in a similar fashion.

3.3. Efficiency of CNT as nucleating agents

A method to quantify the efficiency of a nucleating agent (NE) has been devised by Fillon et al. [69] by comparing the crystallization temperatures of samples with and without the additive under consideration with the crystallization temperature of an ideally self-nucleated neat sample according to:

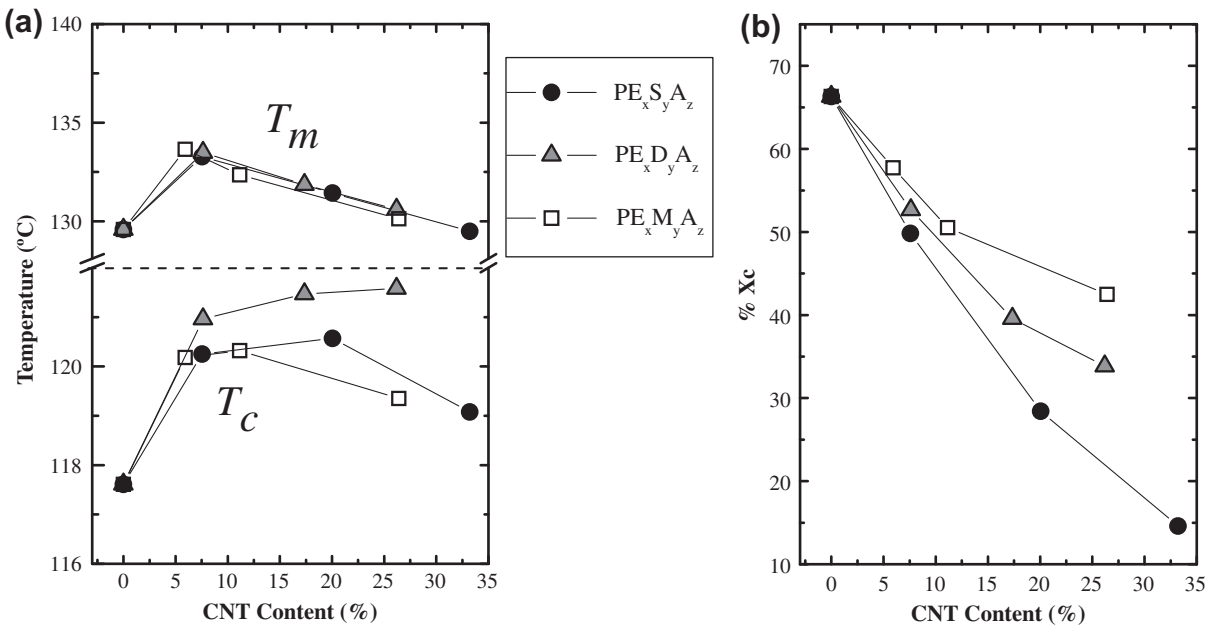

Fig. 4. (a) Crystallization (T_c) and melting peak temperatures (T_m) and (b) crystallinity degree, for the HDPE/CNT nanocomposites as function of the CNT content. Adapted from Refs. [13,14].

$$NE = \frac{T_{c_{NA}} - T_{c_{Polymer}}}{T_{c_{Max\_Polymer}} - T_{c_{Polymer}}} 100 \quad (1)$$

where $T_{c_{NA}}$ is the peak crystallization temperature of the polymer with the nucleating agent, $T_{c_{Polymer}}$ is the peak crystallization temperature of the neat homopolymer (HPDPE, PCL or PEO), and $T_{c_{Max\_Polymer}}$ is the maximum crystallization temperature of the ideally self-nucleated neat homopolymer sample (the ideal self-nucleation temperatures employed were 119.1 °C for HPDE, 32.8 °C for PCL, and 48.4 °C for PEO). The ideal self-nucleation temperature was experimentally determined following the procedure outlined in the experimental part, and it involves producing self-seeds in a sample that is previously crystallized and then heated to a temperature where most of the polymer melts but self-nuclei are produced. The self-nuclei are usually considered to be the best nucleating agents for the polymer under consideration because they have the ideal crystallography for epitaxial nucleation, and this explains why the scale of nucleation efficiency is based on a comparison with the crystallization temperature produced by self-nuclei [14,15,69].

Fig. 5 summarizes the CNT nucleation efficiency for the three polymer matrices evaluated. The efficiency calculated with Eq. (1) yields values above 100% in all cases depicted in Fig. 5, indicating that the CNTs are much better nucleating agents than the homopolymer self-nuclei. Because of this reason we shall refer to this nucleating effect of the CNT's as "super-nucleation".

The trends regarding the type of nanocomposite and the type of CNT employed are not so clear. If we compare nanocomposites made with MWNT's only, the nucleation efficiency is higher for the MWNT-*g*-PCL sample (sample with the lowest CNT content, approximately 2 wt.%), followed by the HDPE/MWNT and MWNT-*g*-PEO samples, respectively. It is tempting to attribute this difference in super-nucleating effects to the grafted (covalently-bonded) nature of the MWNT within the PCL matrix, however, in the case of the PEO, the MWNT are also covalently bonded. Therefore, at the present moment the differences in super-nucleation effect are not completely clear.

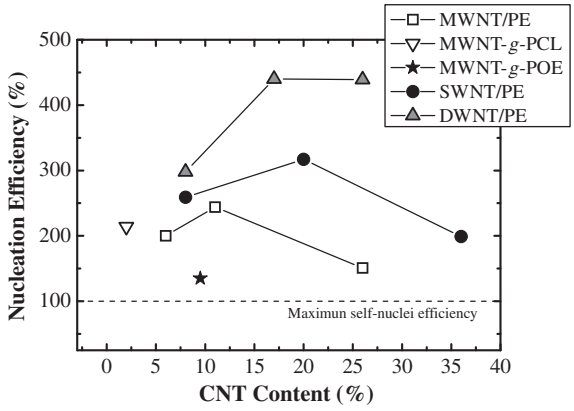

Fig. 5. Efficiency of carbon nanotubes as nucleating agent for several matrices. The estimated experimental error of each data point is less than 3%.

Similarly, when the effect of the nature of the CNTs (multi versus double versus single-wall) upon the nucleation efficiency is evaluated from Fig. 5 another result difficult to explain is obtained. The DWNT fillers display the higher values of nucleation efficiency for the HDPE matrix (from 290% to more than 400%), followed by the SWNT and the MWNT. Based on their surface area, one would expect a higher efficiency for the SWNT. In fact several other results obtained here do indicate a correlation between surface area and nucleation, confinement and crystallization kinetics. Therefore, this particular trend is difficult to understand.

Finally, a maximum in efficiency is observed in a couple of case in Fig. 5 where data with different CNT content was obtained. The trend would have to be validated with more data points, however, if the trend is confirm it would be online with above mentioned competence between super-nucleation and confinement effects at large CNT's content.

Even though the individual trends in the self-nucleation experiments are somewhat controversial, the most important result to be highlighted from this section is the occurrence in all cases of the super-nucleation effect (i.e., nucleating efficiencies larger than 100%). Such effect is probably due to the fact that the polymer chains in all these cases have one end tethered on the surface of the carbon nanotubes thereby facilitating its nucleation on them.

3.4. Isothermal crystallization kinetics

The isothermal crystallization kinetics has been determined by DSC, therefore it corresponds to an overall transformation process that includes both nucleation and growth. The inverse of $\tau_{50\%}$ (i.e., the time needed for 50% relative overall crystallization or half-crystallization time) represents a quantitative measure of the overall crystallization rate. The variation of this overall crystallization rate as a function of crystallization temperature has been plotted in Fig. 6 for the nanocomposites employed here. A modified version of the Lauritzen and Hoffman theory applied to the overall crystallization data was used to fit the experimental data points (the solid lines represent the fit to the theory in Fig. 6). The equation employed was [75–77]:

$$\frac{1}{\tau_{50\%}}(T) = G_o^{\tau} \exp\left(-\frac{U^*}{R(T_c - T_\infty)}\right) \exp\left(-\frac{K_g^{\tau}}{T\Delta T f}\right) \quad (2)$$

where $\tau_{50\%}$ is the overall crystallization half-time determined from DSC measurements. The inverse of $\tau_{50\%}$ represents a measure of the overall crystallization rate that takes into account both nucleation and growth. G_0^{τ} is the overall growth rate constant, U^* is the activation energy for the transport of the chains to the growing nuclei (a value of 1500 cal/mol is usually employed), R is the gas constant and T_c the isothermal crystallization temperature. T_∞ is the temperature at which chain mobility ceases and it is usually taken as $T_g - 30$ (K). ΔT is the supercooling defined as $(T_m^0 - T_c)$, where T_m^0 is the equilibrium melting point. The factor f is a temperature correction term equal to:

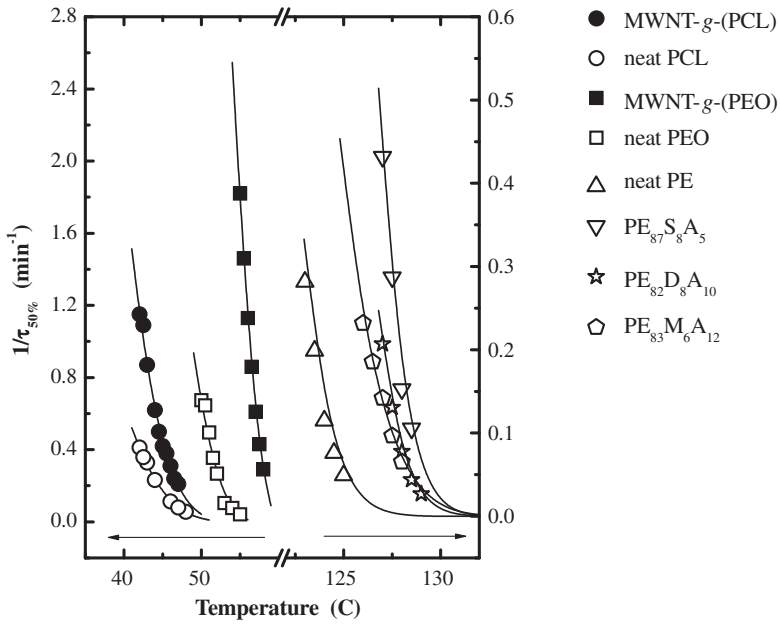

Fig. 6. Overall crystallization rate expressed as the inverse of the half-crystallization time as a function of isothermal crystallization temperature for the indicated samples. Solid lines: Lauritzen–Hoffman theory fit. Adapted from Refs. [13–15].

$2T_c/(T_c + T_m^0)$; and K_g^τ is a term proportional to the energy barrier for the overall crystallization process.

Fig. 6 shows the overall crystallization rate expressed as the inverse of the half-crystallization time as a function of isothermal crystallization temperature for low-CNT content samples (CNT contents below 10 wt.%). For all the cases shown in Fig. 6, the crystallization rate decreases as T_c increases as expected since the crystallizations kinetics is dominated by nucleation (in this case both primary and secondary nucleation) in the temperature regions close to T_m.

The neat HDPE sample needs a much larger supercooling than the HDPE/CNT nanocomposite materials in order to crystallize. The acceleration of the overall crystallization kinetics exhibited by the HDPE/CNT nanocomposites samples is due to the super-nucleation effect of CNT on the HDPE matrix, as it was previously explained. When the HDPE/CNT nanocomposite materials are compared, the following order in overall crystallization rate can be observed: HDPE/SWNT > HDPE/DWNT > HDPE/MWNT. This order reflects the surface area interaction between the different types of CNT and HDPE and therefore their nucleating action, as expected the CNT with the larger exposed area per unit volume is the SWNT, followed by the DWNT and MWNT [13,14]. A similar trend was found in the comparison of the MWNT-*g*-PCL and MWNT-*g*-PEO with their respective homopolymer analogs. The isothermal crystallization kinetics of the grafted PCL and PEO was substantially accelerated as compared to the neat polymers [15]. This strong impact on the nucleation and crystallization kinetics is attributed to the covalent bonding in between the polymers and the MWNT's.

Analyzing the overall crystallization behavior for the HDPE/CNT composites taking into consideration the full CNT content range evaluated (from approx. 6 wt.% until 36 wt.% CNT content), a different behavior can be observed. Fig. 7 shows the overall crystallization rate expressed as the inverse of half-crystallization time and the crystallinity degree as a function of CNT content at a constant isothermal crystallization temperature of 127 °C.

Once more, a competition between super-nucleation and confinement can be observed. At low-CNT contents, super-nucleation dominates and the overall crystallization rate increases with CNT content (a similar result to that observed in Fig. 6). However, at CNT contents above roughly 10% a maximum is observed in the crystallization rate (Fig. 7a) and a decrease in its value at even larger CNT content. The maximum and decrease in crystallization rate are clear indications that confinement effects are taking over the trend at large CNT contents. A similar situation can be observed in Fig. 7b where the crystallinity degree increases above the value achieved by neat HDPE as long as the CNT content is below 10%. Above 10% a sharp decrease in crystallinity degree is observed and extremely low values were obtained for the maximum CNT contents employed (i.e., crystallinity values below 5%). No clear trend was observed regarding the type of CNT in this case.

The energy barrier associated to the overall crystallization kinetics is proportional to K_g^τ (see Eq. (2)) and it is presented in Fig. 8 for all the nanocomposites in consideration with low-CNT content. Only samples with low-CNT contents are presented, since in these samples the super-nucleation effect dominates the overall crystallization rate as explained above (see Fig. 6). Fig. 8 shows that the K_g^τ values are lower in the nanocomposites as compared to the values exhibited by the neat homopolymers. This clear reduction on the K_g^τ values, regardless of the system employed (PCL, PEO or HDPE), corroborates the important

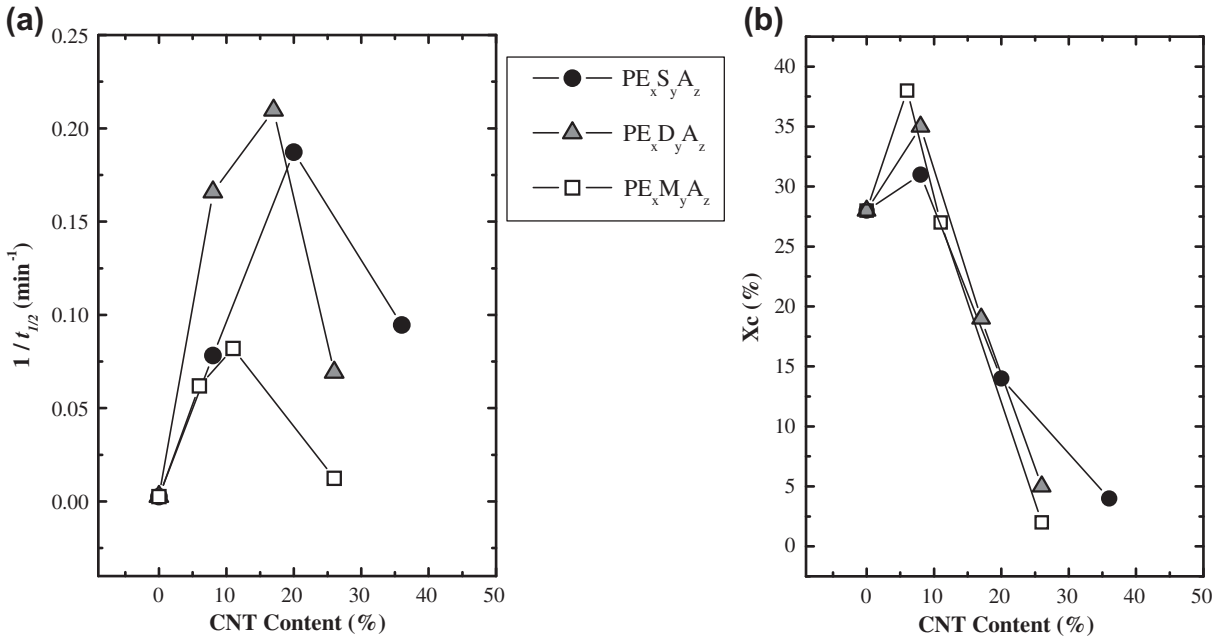

Fig. 7. (a) Overall crystallization rate expressed as the inverse of the half-crystallization time and (b) crystallinity degree as a function of CNT content at a constant isothermal crystallization temperature of 127 °C, for the HDPE/CNT composites. Adapted from Refs. [13,14].

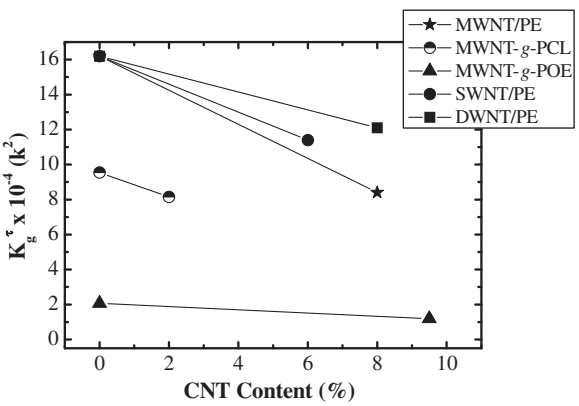

Fig. 8. Variation of the energy barrier for the overall crystallization process, expressed as K_g^τ, for the CNT nanocomposite samples.

super-nucleation effect caused by the CNTs upon the polymer matrix overall crystallization event.

Coming back to the morphological confinement experienced by the PCL phase within linear and miktoarm star copolymers, Fig. 9 shows that the degree of supercooling needed for PCL crystallization increases with the content of PS in the copolymers. Furthermore, the PCL component within the miktoarm star block copolymers needs much larger supercoolings for crystallization than the PCL component within the analog linear diblock copolymers at similar PCL contents. This result confirms that miktoarm molecular architecture causes much larger confinement effects at similar PCL contents when compared to linear analog diblock copolymers. Fig. 9 also shows that in the PCL-containing copolymers (miktoarm and diblocks) where confinement is highest (cylinders and spheres morphologies) the overall crystallization rates are strongly affected, a clear evidence of the high degree of confinement upon the overall crystallization of the PCL component in comparison with neat PCL. In fact in the case of cylinder or sphere forming materials, the overall crystallization had to be determined by the "isothermal step crystallization" technique, since their crystallization was so slow that conventional isothermal DSC can not be employed [32]. When the K_g^τ values obtained from the Lauritzen and Hoffman fittings were examined, the results indicated that as confinement increased, larger K_g^τ values were obtained (see Ref. [12] for more details).

Another way to model the overall isothermal crystallization kinetics is to employ the theory developed by Avrami. The Avrami equation [78,79] can be written as:

$$1 - V_c(t - t_o) = \exp(-k(t - t_o)^n) \quad (3)$$

where: V_c is the relative volumetric transformed fraction (i.e., relative amount of material that has crystallized), n is the Avrami index and k the overall crystallization rate constant (i.e., it contains contributions from both nucleation and growth) and t_o is the induction time. The fit to Eq. (1) was performed in the range 3–25% where correlation coefficients of at least 0.9999 were obtained. For error assessment involved in the Avrami fit the reader is referred to Ref. [79] since we have closely followed the recommended guidelines presented in that reference. It was observed that the fits described the experimental data (results not presented) reasonably well even until 50% conversion (i.e., during the primary crystallization range).

Fig. 10a presents the values of the Avrami indexes obtained as a function of temperature for all the

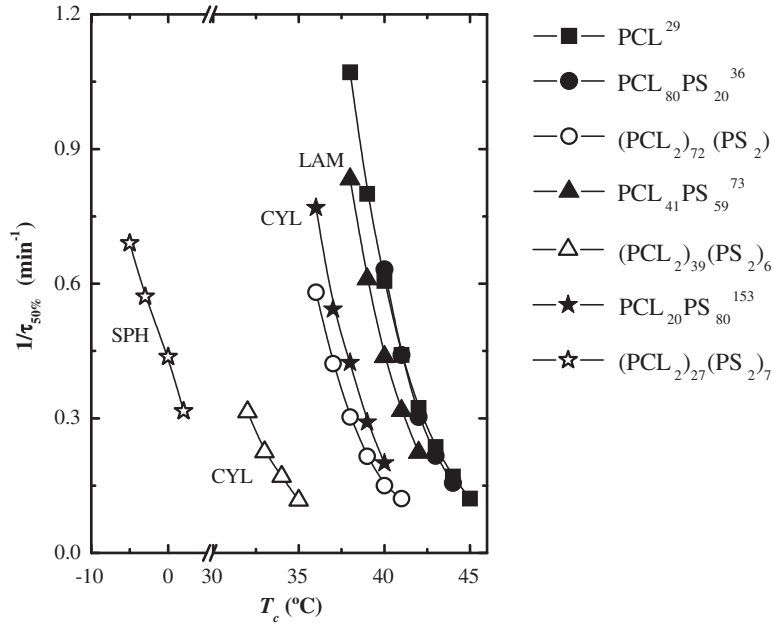

Fig. 9. Overall crystallization rate expressed as the inverse of the half-crystallization time as a function of isothermal crystallization temperature for the linear PCL-*b*-PS diblock copolymers and (PCL_2)-*b*-(PS_2) miktoarm star copolymers. Morphologies: LAM (Lamellar), CYL (Cylinders) and SPH (Spheres). Solid lines: Lauritzen–Hoffman theory fit. Adapted from Ref. [12].

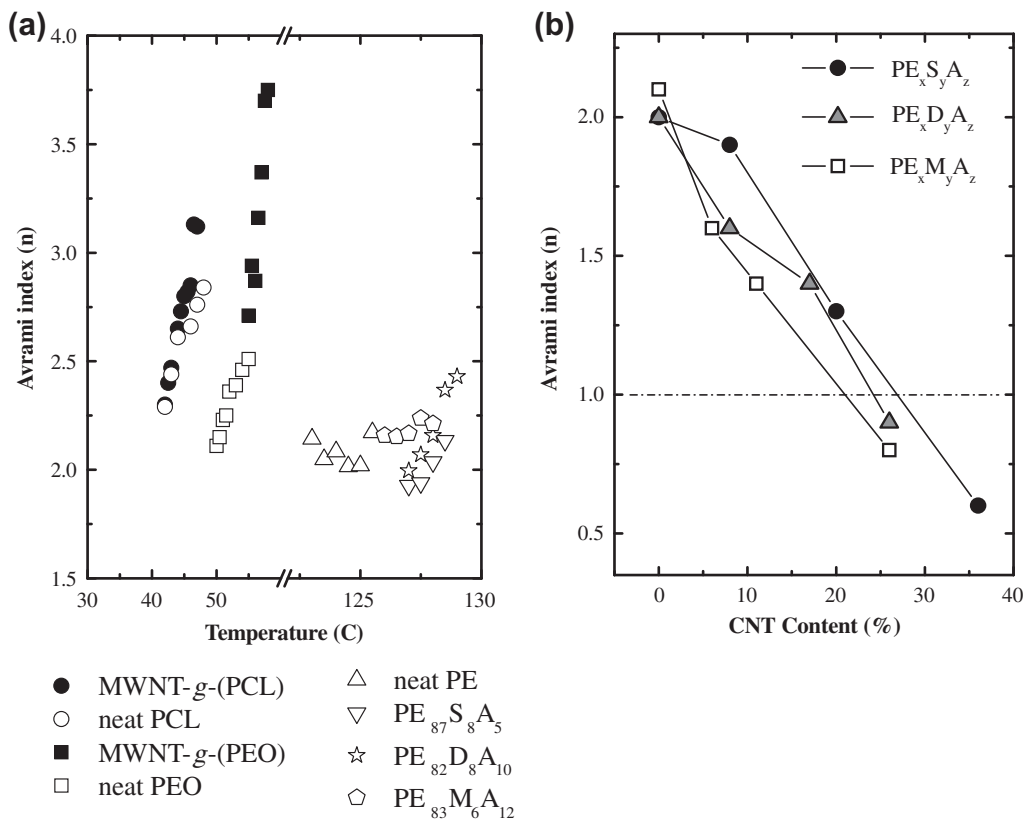

Fig. 10. (a) Avrami index values as a function of isothermal crystallization temperature for the indicated samples, and (b) Avrami index values as function of the CNT content for the HDPE/CNT nanocomposites, at a constant crystallization temperature of 127 °C. Adapted from Ref. [13–15].

nanocomposites with low-CNT contents. For the HDPE/CNT nanocomposites, the Avrami index fluctuates in between 1.9 and 2.4. This corresponds approximately to an Avrami index of 2 which can be interpreted as arising from the instantaneous nucleation of bidimensional structures (e.g., axialites), a result which is consistent with the high density of nuclei present in the neat HDPE employed and further increased by CNT super-nucleation. A bottled brush morphology as well as row nucleated structures would be consistent with two dimensional packing of lamellae that would give rise to Avrami indexes of 2, as in this case.

Likewise, for the PCL and PEO samples grafted to MWNT's, the values of the Avrami index were not greatly affected by the MWNTs inclusion since they were already quite low. An Avrami index value of approximately 2.5–3 indicates instantaneous nucleation of spherulitic structures.

Fig. 10b shows the Avrami index values as a function of the CNT content (up to high CNT contents) for the HDPE/CNT nanocomposites determined at a constant crystallization temperature of 127 °C. The Avrami index strongly reduces as the CNT content increases at a constant T_c temperature until it reaches values of 1 or even lower than 1. This is a remarkable result. As the CNT content increases a network of highly percolated CNT's is created (due mainly to the low percolation threshold) that has a strong interaction with the HDPE chains because of the peculiar morphology induced by the in situ polymerization. We believe that this result is closely linked to the increasing topological confinement caused by the MWNT's on the HDPE matrix. If the confinement is so large, then the primary nucleation will be the rate determining step. This can cause a first order crystallization kinetics in the HDPE matrix or the equivalent of having an Avrami index of 1. A change from nucleation and growth kinetics to a purely nucleation kinetics control occurs when the content of CNT is higher than approximately 10%. Avrami indexes lower than one are produced when the nucleation changes from instantaneous (with $n = 1$) to more sporadic [1]. First order crystallization kinetics also occurs in confined diblock copolymers where isolated phases, like spheres are produced (as it can be seen for the PCL containing miktoarm copolymers evaluated in this work in Fig. 11) [4,12]. The link between the two cases is the confinement of polymer chains. In nanocomposites, the confinement is due to topological restrictions provoked by chain interactions with the nano-filler. On the other hand, in the block copolymers case, the confinement occurs because of the isolated nature of the nanophases produced. The number density of nanodomains (like spheres or cylinders) will be orders of magnitude larger than the heterogeneities content in a bulk homopolymer. Therefore, fractionated crystallization or even homogeneous nucleation can be expected with the concomitant change in crystallization kinetics to a nucleation dominated process [1–4,35].

The Avrami index trend as a function of crystallization temperature for the PCL-containing copolymers can be observed in Fig. 11. The Avrami index increases markedly with T_c when the PCL content within the copolymers samples is nearly 40 wt.% (also for the PCL homopolymer). Such a trend has been reported in the literature for PCL and many other polymers and it has been related to changes in the nucleation mechanism from instantaneous to sporadic nucleation when growth dimensionality is kept constant [75,76]. When the PCL content is low (confined PCL copolymer samples) the Avrami index values are not so sensitive to changes in T_c, they kept almost at a constant value.

When the PCL content within the copolymer samples is below 40 wt.%, the Avrami index exhibits a decreasing trend as the PCL content within the samples decreases.

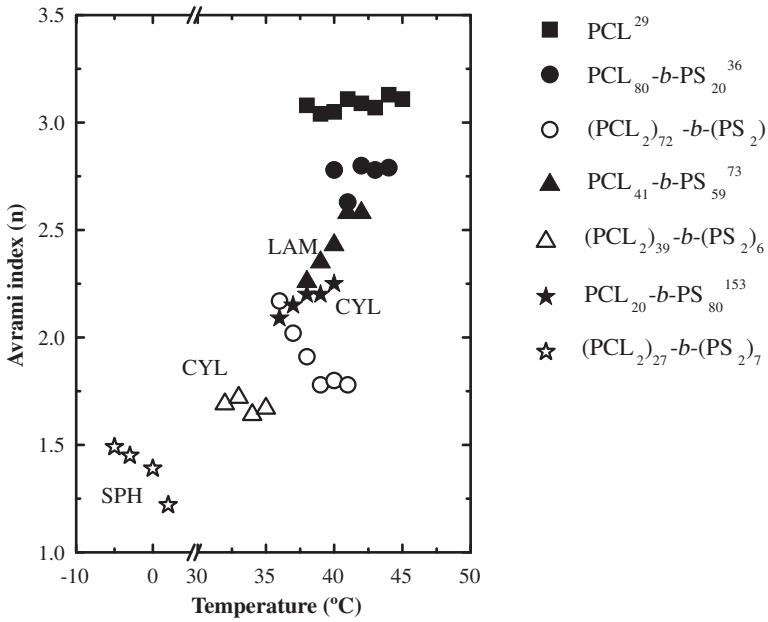

Fig. 11. Avrami index values as a function of isothermal crystallization temperature for linear PCL-*b*-PS diblock copolymers and (PCL_2)-*b*-(PS_2) miktoarm star copolymers. Morphologies: LAM (Lamellar), CYL (Cylinders) and SPH (Spheres). Adapted from Ref. [12].

There is a clear correlation between a decrease in the Avrami index and an increase in the confinement level. The observed shifting in T_c range is an additional evidence of these topological restrictions, since the higher the confinement degree, the larger the supercooling (lower T_c range) needed for the crystallization of the PCL component.

Recently, a comparison between the miktoarm stars and the linear block copolymers was performed and three important effects were found [12]:

(i). a decrease in Avrami index was found due to the morphological change at similar compositions when comparing linear vs. miktoarm star block copolymers;
(ii). if similar morphologies are considered the Avrami index also decreased in the miktoarm star copolymers as compared to the linear ones; and,
(iii). when the PCL component is highly confined (PCL content below 30 wt.%) Avrami indexes between 1.5 and 1 were found. These results indicate that crystallization could start from superficial or homogeneous nucleation phenomena because of the higher supercooling needed for crystallization, see the discussion of Fig. 10.

As shown in this section, the two very different types of confinement present in nanocomposites and in phase segregated block copolymers lead to similar effects from the crystallization kinetics point of view (if we exclude the super-nucleation effect that can dominate the behavior of nanocomposites at low-CNT contents). In both types of materials, confinement reduces the crystallization rates, increases the supercooling needed for crystallization and can even reduce the Avrami index to levels where first order overall crystallization kinetics are produced.

4. Conclusions

A "super-nucleation" effect has been demonstrated for all the nanocomposites studied here. We have employed the term super-nucleation because the CNTs perform a more efficient nucleating action than the self-nuclei of the polymer matrix (self-nuclei are usually considered to be the best nucleating agents for the polymer under consideration). It is believed that such a super-nucleation effect stems from the fact that the polymer chains are tethered to the surface of the CNT and can easily form nuclei. The super-nucleation effect is maximum at low-CNT contents.

The $(PS)_2$-*b*-$(PCL)_2$ miktoarm star copolymers were found to display more compact morphologies for equivalent compositions than linear PS-*b*-PCL diblock copolymers. As a consequence, the crystallization of the PCL component always experiences much higher confinement in the miktoarm stars case than in the linear diblock copolymer case.

The origin of the confinement effect is different in each case. For nanocomposites, confinement is created at high nano-filler loadings because of the interactions between the polymer chains and the extremely large surface area of the carbon nanotubes. In the case of the block copolymers that phase segregate in the melt, the segregation strength produces a very large number of isolated microdomains, such as cylinders or spheres as the content of the non-crystallizable PS component increases. The number of MDs is several orders of magnitude larger than the existing heterogeneities in the copolymer and therefore interfacial or homogeneous nucleation set in.

For nanocomposites a clear competition between super-nucleation and confinement was detected and the behavior is dominated by one or the other depending on the nano-filler content. At low contents the super-nucleation effect dominates the thermal response of the material.

The confinement increases in the nanocomposites as the CNT content increases, and in the block copolymers as the PS content increases. The consequences of confinement are the same in both cases even if the origin of the phenomena is different in each case. During non-isothermal DSC experiments, a reduction of both crystallization and melting temperatures and a strong reduction of the crystallinity degree was observed when confinement dominates the behavior. Changes are even more dramatic when isothermal crystallization is considered since confinement causes a depression of the overall crystallization rate and a decrease in the Avrami index until values of one or lower are achieved indicating a nucleation control on the overall crystallization kinetics. The energy barrier for primary and secondary crystallization was calculated and it increases as confinement increases. However, for the nanocomposites, at low-CNT contents where the behavior is dominated by super-nucleation, the energy barrier for nucleation decreases as compared to the homopolymer.

Acknowledgments

We would like to thank professors Nikos Hadjichristidis and Philippe Dubois for their contributions in the synthesis of the interesting polymeric materials that we have jointly investigated in the past few years. We would also like to acknowledge the contribution of professors Hsin-Lung Chen and Ian Hamley for their invaluable help in the X-ray characterization of these block copolymers and nanocomposites.

References

[1] Müller AJ, Balsamo V, Arnal ML. Nucleation and crystallization in diblock and triblock copolymers. Adv Polym Sci 2005;190:1–63.
[2] Müller AJ, Arnal ML, Balsamo V. Crystallization in block copolymers with more than one crystallizable block. In: Reiter G, Strobl GR, editors. Progress in understanding of polymer crystallization. Berlin: Springer-Verlag; 2007. p. 229–59.
[3] Castillo RV, Müller AJ. Crystallization and morphology of biodegradable or biostable single and double crystalline block copolymers. Prog Polym Sci 2009;34(6):516–60.
[4] Loo YL, Register RA. Crystallization within block copolymer mesophases. In: Hamley IW, editor. Developments in block copolymer science and technology. New York: John Wiley & Sons, Inc.; 2004. p. 213–43.
[5] Hamley IW. The physics of block copolymers. Oxford: Oxford University Press; 1998.
[6] Ajayan PM. In: Naiwa HS, editor. Handbook of nano-structured materials and nanotechnology. New York: Academic Press; 2000.

[7] Wang C, Guo Z-X, Fu S, Wu W, Zhu D. Polymers containing fullerene or carbon nanotube structures. Prog Polym Sci 2004;29(11): 1079–141.
[8] Ajayan PM, Zhou OZ. Applications of carbon nanotubes. Top Appl Phys 2001;80:391–425.
[9] Moniruzzaman M, Winey KI. Polymer nanocomposites containing carbon nanotubes. Macromolecules 2006;39(16):5194–205.
[10] Bonduel D, Alexandre M, Monteverde F, Dubois P, Mainil M. Supported coordination polymerization: a unique way to potent polyolefin carbon nanotube nanocomposites. Chem Commun 2005;6:781–3.
[11] Lorenzo AT, Müller AJ, Priftis D, Pitsikalis M, Hadjichristidis N. Synthesis and morphological characterization of miktoarm star copolymers (PCL)(2)(PS)(2) of poly(epsilon-caprolactone) and polystyrene. J Polym Sci Part A: Polym Chem 2007;45(23): 5387–739.
[12] Lorenzo AT, Müller AJ, Lin M-C, Chen H-L, Jeng U-S, Priftis D, et al. Influence of macromolecular architecture on the crystallization of (PCL2)-*b*-(PS2) 4-miktoarm star block copolymers in comparison to linear PCL-*b*-PS diblock copolymer analogues. Macromolecules 2009;42(11):8353–64.
[13] Trujillo M, Arnal ML, Müller AJ, Laredo E, Bredeau St, Bonduel D, et al. Thermal and morphological characterization of nanocomposites prepared by in situ polymerization of high density polyethylene on carbon nanotubes. Macromolecules 2007;40(17):6268–76.
[14] Trujillo M, Arnal ML, Müller AJ, Bredeau St, Bonduel D, Dubois Ph, et al. Thermal fractionation and isothermal crystallization of polyethylene nanocomposites prepared by in situ polymerization. Macromolecules 2008;41(6):2087–95.
[15] Priftis D, Sakellariou G, Hadjichristidis N, Penott EK, Lorenzo AT, Müller AJ. Surface modification of multiwalled carbon nanotubes with biocompatible polymers via ring opening and living anionic surface initiated polymerization. Kinetics and crystallization behaviour. J Polym Sci Part A: Polym Chem 2009;47(17):4379–90.
[16] Hadjichristidis N, Pispas S, Floudas G. Block copolymers: synthetic strategies, physical properties, and applications. United Kingdom: Wiley; 2002.
[17] Hadjichristidis N, Iatrou H, Pitsikalis M, Pispas S, Avgeropoulos A. Linear and non-linear triblock terpolymers. Synthesis, self-assembly in selective solvents and in bulk. Prog Polym Sci 2005;30(7): 725–82.
[18] Lee W, Chen HL, Lin TL. Correlation between crystallization kinetics and microdomain morphology in block copolymer blends exhibiting confined crystallization. J Polym Sci Part B: Polym Phys 2002;40(6):519–29.
[19] Rangarajan P, Register RA, Adamson DH, Fetters LJ, Bras W, Naylor S, et al. Dynamics of structure formation in crystallizable block copolymers. Macromolecules 1995;28(5):1422–8.
[20] Mai SM, Fairclough JPA, Viras K, Gorry PA, Hamley IW, Ryan AJ, et al. Chain folding in semicrystalline oxyethylene/oxybutylene diblock copolymers. Macromolecules 1997;30(26):8392–400.
[21] Nojima S, Kato K, Yamamoto S, Ashida T. Crystallization of block copolymers. 1. Small-angle X-ray scattering study of ε-caprolactone-butadiene diblock copolymer. Macromolecules 1992;25(8): 2237–42.
[22] Zhu L, Calhoun BH, Ge Q, Quirk RP, Cheng SZD, Thomas EL, et al. Initial-stage growth controlled crystal orientations in nanoconfined lamellae of a self-assembled crystalline-amorphous diblock copolymer. Macromolecules 2001;34(5):1244–51.
[23] Kofinas P, Cohen RE. Morphology of highly textured poly(ethylene)/poly(ethylene-propylene) (E/EP) semicrystalline diblock copolymers. Macromolecules 1994;27(11):3002–8.
[24] Hong S, Yang L, MacKnight WJ, Gido SP. Morphology of a crystalline/amorphous diblock copolymer: poly((ethylene oxide)-b-butadiene). Macromolecules 2001;34(20):7009–16.
[25] Reiter G, Castelein G, Sommer JU, Rottele A, Thurn-Albrecht T. Direct visualization of random crystallization and melting in arrays of nanometer-size polymer crystals. Phys Rev Lett 2001;87(22): 226101–4.
[26] Chen HL, Li HC, Huang YY, Chiu FC. Crystallization-induced deformation of spherical microdomains in block copolymer blends consisting of a soft amorphous phase. Macromolecules 2002;35(6): 2417–22.
[27] Loo YL, Register RA, Ryan AJ, Dee GT. Polymer crystallization confined in one, two, or three dimensions. Macromolecules 2001;34(26):8968–77.
[28] Loo YL, Register RA, Ryan AJ. Modes of crystallization in block copolymer microdomains: breakout, templated, and confined. Macromolecules 2002;35(6):2365–74.
[29] Loo YL, Register RA, Ryan AJ. Polymer crystallization in 25-nm spheres. Phys Rev Lett 2000;84(18):4120–3.
[30] Loo YL, Register RA, Adamson DH. Polyethylene crystal orientation induced by block copolymer cylinders. Macromolecules 2000; 33(21):8361–6.
[31] Balsamo V, Paolini Y, Ronca G, Müller AJ. Crystallization of the polyethylene block in polystyrene-b-polyethylene-b-polycaprolactone triblock copolymers, 1. Self-nucleation behavior. Macromol Chem Phys 2000;201(18):2711–20.
[32] Balsamo V, Urdaneta N, Pérez L, Carrizales P, Abetz V, Müller AJ. Effect of the polyethylene confinement and topology on its crystallization within semicrystalline ABC triblock copolymers. Eur Polym J 2004;40(6):1033–49.
[33] Lorenzo AT, Arnal ML, Müller AJ, Boschetti de Fierro A, Abetz V. Confinement effects on the crystallization and SSA thermal fractionation of the PE block within PE-b-PS diblock copolymers. Eur Polym J 2006;42(3):516–33.
[34] Lorenzo AT, Arnal ML, Müller AJ, Boschetti de Fierro A, Abetz V. Nucleation and isothermal crystallization of the polyethylene block within diblock copolymers containing polystyrene and poly(ethylene-alt-propylene). Macromolecules 2007;40(14):5023–37.
[35] Müller AJ, Balsamo V, Arnal ML, Jakob T, Schmalz H, Abetz V. Homogeneous nucleation and fractionated crystallization in block copolymers. Macromolecules 2002;35(8):3048–58.
[36] Albuerne J, Márquez L, Müller AJ, Raquez JM, Degée Ph, Dubois Ph, et al. Nucleation and crystallization in double crystalline poly(p-dioxanone)-b-poly(ε-caprolactone) diblock copolymers. Macromolecules 2003;36(5):1633–44.
[37] Müller AJ, Albuerne J, Márquez L, Raquez JM, Degée Ph, Dubois Ph, et al. Self-nucleation and crystallization kinetics of double crystalline poly(p-dioxanone)-b-poly(ε-caprolactone) diblock copolymers. Faraday Discuss 2005;128:231–53.
[38] Hamley W, Castelletto V, Castillo RV, Müller AJ, Martin CM, Pollet E, et al. Crystallization in poly(l-lactide)-b-poly(ε-caprolactone) double crystalline diblock copolymers: a study using X-ray scattering, differential scanning calorimetry, and polarized optical microscopy. Macromolecules 2005;38(2):463–72.
[39] Hamley IW, Parras P, Castelletto V, Castillo RV, Müller AJ, Pollet E, et al. Melt structure and its transformation by sequential crystallization of the two blocks within poly(L-lactide)-block-poly(-caprolactone) double crystalline diblock copolymers. Macromol Chem Phys 2006;207(11):941–53.
[40] Olvera de la Cruz M, Sanchez IC. Theory of microphase separation in graft and star copolymers. Macromolecules 1986;19(10):2501–8.
[41] Milner ST. Chain architecture and asymmetry in copolymer microphases. Macromolecules 1994;27(8):2333–5.
[42] Zhu Y, Gido SP, Moshakou M, Iatrou H, Hadjichristidis N, Park S, et al. Effect of junction point functionality on the lamellar spacing of symmetric (PS)n(PI)n miktoarm star block copolymers. Macromolecules 2003;36(15):5719–24.
[43] Olmsted PD, Milner ST. Strong segregation theory of bicontinuous phases in block copolymers. Macromolecules 1998;31(12):4011–22.
[44] Buzza DMA, Hamley IW, Fzea AH, Moniruzzaman FM, Allgaier JB, Young RN, et al. Comparing a symmetric diblock copolymer AB with its hetero-four-arm star analog A2B2. Macromolecules 1999;32(22):7483–95.
[45] Floudas G, Hadjichristidis N, Iatrou H, Pakula T, Fischer EW. Microphase separation in model 3-miktoarm star copolymers (simple graft and terpolymers). 1. Statics and kinetics. Macromolecules 1994;27(26):7735–46.
[46] Beyer FL, Gido SP, Uhrig D, Mays JW, Tan NB, Trevino SF. Morphological behavior of A2B2 star block copolymers. J Polym Sci Part B: Polym Phys 1999;37(24):3392–400.
[47] Beyer FL, Gido SP, Velis G, Hadjichristidis N, Tan NB. Morphological behavior of A5B miktoarm star block copolymers. Macromolecules 1999;32(20):6604–7.
[48] Grayer V, Dormidontova EE, Hadziioannou G, Tsitsilianis C. A comparative experimental and theoretical study between heteroarm star and diblock copolymers in the microphase separated state. Macromolecules 2000;33(17):6330–9.
[49] Matsen MW, Gardiner JM. Anomalous domain spacing difference between AB diblock and homologous A2B2 starblock copolymers. J Chem Phys 2000;113(5):1673–2048.
[50] Kaminsky W, Zielonka H. Polymerization of olefins in the presence of metal powders with homogeneous catalysts. Polym Adv Technol 1993;4(7):415–22.
[51] Alexandre M, Martin E, Dubois P, Garcia-Marti M, Jérôme R. Use of metallocenes in the polymerization-filling technique with production of polyolefin-based composites. Macromol Rapid Commun 2000;21(13):931–6.

[52] Alexandre M, Martin E, Dubois P, Garcia-Marti M, Jérome R. Polymerization-filling technique: an efficient way to improve the mechanical properties of polyethylene composites. Chem Mater 2001;13(2):236–7.
[53] Alexandre M, Pluta M, Dubois P, Jérôme R. Metallocene catalyzed polymerization of ethylene in the presence of graphite, 1. Synthesis and characterization of the composites. Macromol Chem Phys 2001;202(11):2239–46.
[54] Mahfuz H, Adnan A, Rangari VK, Jeelani S. Manufacturing and characterization of carbon nanotube/polyethylene composites. Int J Nanosci 2005;4(1):55–72.
[55] Haggenmueller R, Fisher JE, Winey KI. Single wall carbon nanotube/polyethylene nanocomposites: nucleating and templating polyethylene crystallites. Macromolecules 2006;39(8):2964–71.
[56] Bhattacharyya AR, Sreekumar TV, Liu T, Kumar S, Ericson LM, Hauge RH, et al. Crystallization and orientation studies in polypropylene/single wall carbon nanotube composite. Polymer 2003;44(8):2373–7.
[57] Assouline E, Lustiger A, Barber AH, Cooper CA, Klein E, Wachtel E, Wagner HD. Nucleation ability of multiwall carbon nanotubes in polypropylene composites. J Polym Sci Part B: Polym Phys 2003;41(5):520–7.
[58] Probst O, Moore EM, Resasco DE, Grady BP. Nucleation of polyvinyl alcohol crystallization by single-walled carbon nanotubes. Polymer 2004;45(13):4437–43.
[59] Minus ML, Chae HG, Kumar S. Single wall carbon nanotube templated oriented crystallization of poly(vinyl alcohol). Polymer 2006;47(11):3705–10.
[60] Michell CA, Krishnamoorti R. Non-isothermal crystallization of in situ polymerized poly(ε-caprolactone) functionalized-SWNT nanocomposites. Polymer 2005;46(20):8796–804.
[61] Ryan KP, Lipson SM, Drury A, Cadek M, Ruether M, O'Flaherty SM, et al. Carbon-nanotube nucleated crystallinity in a conjugated polymer based composite. Chem Phys Lett 2004;391(4–6):329–33.
[62] Bao SP, Tjong SC. Mechanical behaviors of polypropylene/carbon nanotube nanocomposites: the effects of loading rate and temperature. Mater Sci Eng: A 2008;485(1–2):508–16.
[63] Anand KA, Agarwal US, Joseph R. Carbon nanotubes induced crystallization of poly(ethylene terephthalate). Polymer 2006;47(11):3976–80.
[64] Gao Y, Wang Y, Shi J, Bai H, Song B. Functionalized multi-walled carbon nanotubes improve nonisothermal crystallization of poly(ethylene terephthalate). Polym Test 2008;27(2):179–88.
[65] Chen EC, Wu TM. Isothermal crystallization kinetics and thermal behavior of poly(ε-caprolactone)/multi-walled carbon nanotube composites. Polym Degrad Stab 2007;92(6):1009–15.
[66] Goh HW, Goh SW, Xu GQ, Pramoda KP, Zhang WD. Crystallization and dynamic mechanical behavior of double-C60-end-capped poly(ethylene oxide)/multi-walled carbon nanotube composites. Chem Phys Lett 2003;379(3–4):236–41.
[67] Chatterjee T, Yurekli K, Hadjiev VG, Krishnamoorti R. Single-walled carbon nanotube dispersions in poly(ethylene oxide). Adv Funct Mater 2005;15(11):1832–8.
[68] Jin J, Song M, Pan F. A DSC study of effect of carbon nanotubes on crystallisation behaviour of poly(ethylene oxide). Thermochim Acta 2007;456(1):25–31.
[69] Fillon B, Whittmann JC, Lotz B, Thierry A. Self-nucleation and recrystallization of isotactic polypropylene (phase) investigated by differential scanning calorimetry. J Polym Sci Part B: Polym Phys 1993;31(10):1383–93.
[70] Arnal ML, Balsamo V, Ronca G, Sánchez A, Müller AJ, Cañizales E, et al. Applications of successive self-nucleation and annealing (SSA) to polymer characterization. J Therm Anal Calorim 2000;59(1–2):451–70.
[71] Müller AJ, Arnal ML. Thermal fractionation of polymers. Prog Polym Sci 2005;30(5):559–603.
[72] Lorenzo AT, Arnal ML, Müller AJ, Boschetti de Fierro A, Abetz V. High speed SSA thermal fractionation and limitations to the determination of lamellar sizes and their distributions. Macromol Chem Phys 2006;207(1):39–49.
[73] Müller AJ, Lorenzo AT, Arnal ML. Recent advances and applications of successive self-nucleation and annealing (SSA) high speed thermal fractionation. Macromol Symp 2009;277(1):207–14.
[74] Lorenzo AT, Arnal ML, Sánchez JJ, Müller AJ. Effect of annealing time on the self-nucleation behavior of semicrystalline polymers. J Polym Sci Polym Phys 2006;44:1738–50.
[75] Mardelkern L. Crystallization of polymer. Kinetics and mechanisms. United Kingdom: Cambridge University Press; 2002.
[76] Strobl G. Crystallization and melting of bulk polymers: new observations, conclusions and a thermodynamic scheme. Prog Polym Sci 2006;31(4):398–442.
[77] Lorenzo AT, Müller AJ. Estimation of the nucleation and crystal growth contributions to the overall crystallization energy barrier. J Polym Sci B Polym Phys 2008;46(14):1478–87.
[78] Avrami M. Granulation, phase change, and microstructure kinetics of phase change. III. J Chem Phys 1941;9(2):177–84.
[79] Lorenzo A, Arnal ML, Albuerne J, Müller AJ. DSC isothermal polymer crystallization kinetics measurements and the use of the Avrami equation to fit the data: guidelines to avoid common problems. Polym Test 2007;26(2):222–31.

Prof. A.J. Müller (born 1960) is a Materials Engineer, with an M.Sc. in Chemistry (1983) and a Ph.D. in Physics (from Bristol University, U.K., 1989). He is presently the head of the Simón Bolívar University polymer group and holds the position of Full Professor in the Materials Science Department. He has co-authored more than 300 publications from which 155 have been published in international peer review journals (indexed in the SCI). He has tutored 82 B.Sc. thesis and 42 postgraduate thesis (both M.Sc. and Ph.D.). He has won several awards in Venezuela, including the Lorenzo Mendoza Fleury, Polar Prize for basic science. Prof. Müller has given keynote, plenary and invited lectures in more than 20 countries around the world. He has achieved an *h index* of **30** (December 2010). In July 2009 he became a "corresponding member" of the Venezuelan National Academy of Engineering and Habitat (ANIH). His field of interests include: polymer solution rheology, structured fluids, morphology, nucleation, crystallization and crystallization kinetics of semi-crystalline materials and of multiphasic materials (in particular polymer blends, block copolymers, biopolymers and nano-composites). He is the current president of the Venezuelan Polymer Association (ASOVENP).

María L. Arnal is a Materials Engineer, with an M.Sc. and Ph.D. in Engineering (from Simón Bolívar University, Venezuela). She currently holds the position of full professor at the Materials Science department of Simón Bolívar University (Caracas, Venezuela). She has co-authored 42 publications which have been published in international peer review journals (indexed in the SCI) achieving an *h-Index* of 18. Fields of interest of María L. Arnal are: i) thermal analysis ii) morphology, nucleation and crystallization behavior of semi-crystalline materials and semi-crystalline components within multiphasic materials (polymer blends, block copolymers and nanocomposites); ii) polymer characterization. In addition she had worked in the paint and coating industry.

Mariselis Trujillo (bord in 1975) is a Materials Engineer from Simón Bolívar University, Venezuela, with a M.Sc. in Engineering and is soon due to complete her Ph.D. studies of Engineering at the same University. She has 5 years of experience in the engineering field, working in the oil industry specifically in the Materials Technology Department of PDVSA Intevep, S.A. (Edo. Miranda, Venezuela). In the last 5 year she has worked in academic activities as a research scientist in polymers science and teacher assistant in the Material Science Department at the Simón Bolívar University (Caracas, Venezuela). Since 2010, she is a junior assistant professor at the Department of Mechanics. Mariselis Trujillós expertise areas include: i) morphology, nucleation and crystallization behavior of semi-crystalline materials and semi-crystalline components within nanocomposites; ii) relationship

between morphology, structure and the rheological and mechanical properties of nanocomposites and iii) processing of thermoplastic polymers and nanocomposites.

Arnaldo T. Lorenzo is a Materials Engineer, with a Ph.D. in Engineering (from Simón Bolívar University, Venezuela). Former assistant professor at the Materials Science department at the Simón Bolívar University (Caracas, Venezuela). Since September 2010 he holds a position as a Post-Doctoral fellow at the department of Chemical and Biomolecular Engineering in the College of Engineering at the University of Houston (Texas, U.S.). He has co-authored 23 publications which have been published in international peer review journals (indexed in the SCI). Arnaldo Lorenzós field of interests include: i) morphology, nucleation and crystallization behavior of semi-crystalline materials and semi-crystalline components within multiphasic materials (polymer blends, block copolymers and nanocomposites); ii) polymer rheology in the bulk and solution state.